Sparse Transfer Response-Based Incoherent OFDR With High Accuracy and Low Overhead

Lihan Wang, *Graduate Student Member, IEEE*, Jingxian Wang, Xi Liu, Haoran Wu, Wei Zhang, Yu Zhang, Yi Shao, Kaiyu Chen, Xiangchuan Wang, *Member, IEEE*, and Shilong Pan, *Fellow, IEEE*

***Abstract*—An incoherent optical frequency domain reflectometry (I-OFDR) method enhanced by orthogonal matching pursuit (OMP) and phase-derived ranging (PDR) is proposed to enable high-accuracy multipath delay measurement with reduced computational complexity. Unlike traditional I-OFDR systems that require continuous linear frequency sweeping, the proposed method performs sparse RF response acquisition and avoids fixed frequency interval constraints inherent in Fourier-based analysis. Experimental results demonstrate that the proposed method achieves sub-picosecond-level multipath transfer delay accuracy while requiring only 10% of the frequency points needed by traditional I-OFDR methods, greatly reducing the signal processing requirement.**

***Index Terms*—Incoherent frequency domain reflectometry, microwave photonics, multipath transfer delay measurement, phase-derived ranging.**

I. Introduction

DISTRIBUTED fiber-optic sensors [1], [2], [3] have gained widespread adoption across multiple engineering fields, particularly in structural health monitoring, perimeter security, and environmental monitoring. These sensing systems operate on the principle of detecting distributed physical parameters along optical fibers through continuous measurement of optical signal characteristics, including intensity variations, phase shifts, and wavelength modulations.

Among various distributed sensing techniques, incoherent optical frequency domain reflectometry (I-OFDR) has emerged as a prominent solution for high-performance distributed sensing, offering low system complexity and broad sensing range. This approach originates from microwave photonic sensing [4], [5], in which an equivalent optical time-domain reflectometry (OTDR) trace can be obtained from the radio frequency (RF) transfer function of the optical link. Unlike broadband pulse detection, I-OFDR achieves a superior signal-to-noise ratio (SNR) by utilizing narrow-bandwidth intermediate frequency (IF) reception in the electrical domain [6].

Received 28 June 2025; revised 31 July 2025; accepted 14 August 2025. Date of publication 19 August 2025; date of current version 25 August 2025. This work was supported in part by the National Natural Science Foundation of China under Grant 62271249 and in part by the Fundamental Research Funds for the Central Universities under Grant NC2024004. *(Corresponding author: Xiangchuan Wang.)*

The authors are with the National Key Laboratory of Microwave Photonics, Nanjing University of Aeronautics and Astronautics, Nanjing 210016, China (e-mail: andwwlh@nuaa.edu.cn; wangxch@nuaa.edu.cn).

Color versions of one or more figures in this letter are available at https://doi.org/10.1109/LPT.2025.3600030.

Digital Object Identifier 10.1109/LPT.2025.3600030

However, the response speed of I-OFDR systems is typically limited because the high SNR achieved by I-OFDR comes at the expense of high-accuracy magnitude-phase detection. Moreover, these methods often rely on algorithms based on Fourier analysis [7], [8], [9], which necessitate that the obtained RF transfer function be both continuous and uniformly sampled. The span of the RF frequency range determines the time-domain resolution, while the RF frequency interval determines the measurement range. Therefore, in measurement scenarios that demand both a large sensing range and high spatial resolution, the measurement time becomes significant. Significant research efforts have been dedicated to reducing the overhead of I-OFDR systems. For instance, [10] employed an adaptive filter to narrow the main lobe of the time-domain response, thereby reducing the required number of RF frequency points. But the RF frequency points must still be set continuously. Reference [11] implemented I-OFDR sensing using a sparse transfer function. However, this approach is predicated on the assumption of equally spaced sensors and cannot be generalized to broader scenarios. Reference [12] utilized a compressed sensing algorithm to minimize the number of frequency points, yet the demodulation process still necessitated sweeping the laser wavelength to resolve the transfer function. To date, I-OFDR still lacks a dedicated method that effectively mitigates the time consumption associated with large-range and high-resolution sensing tasks.

In this Letter, we propose an I-OFDR demodulation method integrating orthogonal matching pursuit (OMP) [13] with phase-derived ranging (PDR) [14]. By utilizing a sparse transfer response, the proposed approach significantly reduces the hardware overhead during the measurement. To further minimize computational overhead at the backend, we employ PDR to compensate for the low-resolution results of OMP, thereby avoiding the traditional Fourier analysis methods that rely on zero-padding or interpolation to enhance measurement accuracy. In the experiments, we applied the proposed method to interrogate the wavelengths of distributed FBGs and multiple lasers. While maintaining sub-picosecond-level multipath transfer delay accuracy, we reduced the required measurement frequency points to just 10% of those needed in fixed frequency interval methods. Moreover, the proposed method effectively decreased the sidelobe interference introduced by the Fourier transform, further enhancing the measurement accuracy of the I-OFDR approach.

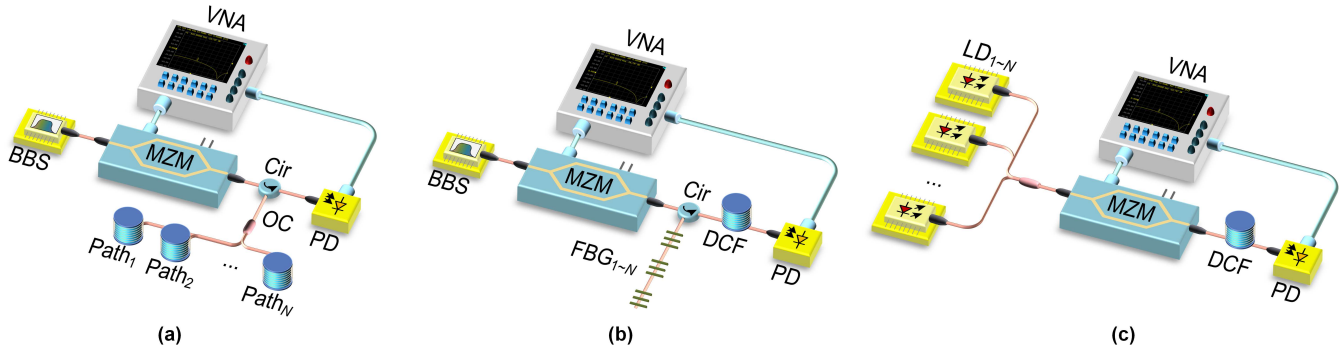

Fig. 1. The diagram of three typical I-OFDR systems. (a) Multipath optical transfer delay measurement. (b) Distributed fiber Bragg grating (FBG) sensing. (c) Multi-wavelength demodulation. BBS, broadband source. MZM, Mach-Zehnder modulator. Cir, optical circulator. OC, optical coupler. PD, photodetector. LD, laser diode. DCF, dispersion compensating fiber. VNA, vector network analyzer.

II. System Model

To illustrate the principle of the proposed OMP-PDR enhanced sparse I-OFDR, we use multipath optical transfer delay measurement as an example. Other I-OFDR configurations used for wavelength sensing, as shown in Figs. 1(b) and 1(c), follow a similar demodulation process based on wavelength-to-delay mapping. The wavelength variation can be calculated from the measured optical transfer delay using the known dispersion relation. In Fig. 1(a), a broadband source, amplitude-modulated by an RF signal with stepped frequency, serves as the optical sensing signal for I-OFDR measurement. After transmission through the optical links under test, which include multiple paths, the envelope of the sensing signal exhibits several corresponding attenuations and phase shifts. Due to the incoherent nature of the measurement, interference between different paths may be neglected, as the coherence time of the broadband source is usually much shorter than the delay difference between paths. Subsequently, the envelope of the optical signal is extracted using a photodetector (PD) through square-law detection. By employing a vector network analyzer (VNA), the transfer response in the I-OFDR can be obtained:

$$H(\omega) = \sum_{l=1}^{L} \alpha_{\mathrm{m},l} e^{-j\omega\tau_{\mathrm{m},l}} \tag{1}$$

where L is the number of measured paths, $\alpha_{\mathrm{m},l}$ and $\tau_{\mathrm{m},l}$ are the insertion loss and transfer delay of the l^{th} path. In conventional methods, Fourier analysis is employed to determine the value of $\tau_{\mathrm{m},l}$. Consequently, the frequency response can be formulated in matrix form as follows:

$$\begin{aligned}\mathbf{H} &= \boldsymbol{\Omega}(\tau)\cdot\mathbf{T} \\ &= [\omega(\tau_1), \omega(\tau_2), \ldots, \omega(\tau_N)]\cdot\mathbf{T} \\ &= \begin{bmatrix} e^{-j\omega_1\tau_1} & e^{-j\omega_1\tau_2} & \cdots & e^{-j\omega_1\tau_N} \\ e^{-j\omega_2\tau_1} & e^{-j\omega_2\tau_2} & \cdots & e^{-j\omega_2\tau_N} \\ \cdots & \cdots & \cdots & \cdots \\ e^{-j\omega_M\tau_1} & e^{-j\omega_M\tau_2} & \cdots & e^{-j\omega_M\tau_N} \end{bmatrix} \cdot \begin{bmatrix} \cdots \\ \alpha_{m,1} \\ \cdots \\ \alpha_{m,L} \\ \cdots \end{bmatrix}\end{aligned} \tag{2}$$

In (2), $\mathbf{H}$ is an $M\times 1$ frequency response vector. The matrix $\Omega(\tau)$ is defined as $[\omega(\tau_1), \omega(\tau_2), \ldots, \omega(\tau_N)]$, which is an $M\times N$ discrete Fourier transform (DFT) matrix. Here, $\omega(\tau_n)$ denotes the phase response corresponding to a link transfer delay of τ_n, and it can be expressed as:

$$\omega(\tau_n) = [e^{j\omega_1\tau_n}, e^{j\omega_2\tau_n}, \ldots, e^{j\omega_M\tau_n}]^H \tag{3}$$

where $[\ldots]^H$ denotes the conjugate transpose operator. In this model, the measurement process is discretized as an $N\times 1$ time-domain response vector $\mathbf{T}$. If the vector $\mathbf{T}$ attains its maximum value at the n^{th} element, we can estimate the transfer delay to be τ_n. Consequently, the problem of multipath delay measurement is reformulated equivalently as:

$$\{\hat{\tau}\} = \left\{ \tau \,\middle|\, \tau_n, n = \underset{n}{\mathrm{argmax}} |\mathbf{T}(n)| \right\} \text{ s.t.} \mathbf{H} = \boldsymbol{\Omega}(\tau)\cdot\mathbf{T} \tag{4}$$

To solve (4), an inverse DFT (iDFT) can be applied to $\mathbf{H}$ to calculate the time-domain response $\mathbf{T}$, as illustrated in the first row of Fig. 2. Using zero-padding in the iDFT or interpolation in the time domain, one can refine the time-delay interval to a smaller scale, thereby enhancing the accuracy. However, the aforementioned demodulation process assumes that the RF frequencies are set with a fixed interval. If we aim to effectively reduce the frequenciy points, a sparse RF response with random intervals will lead to significant interference after the iDFT. The sparse RF response can be conceptualized as a full transfer function multiplied by a random sampling pattern, as depicted in the second row of Fig. 2.

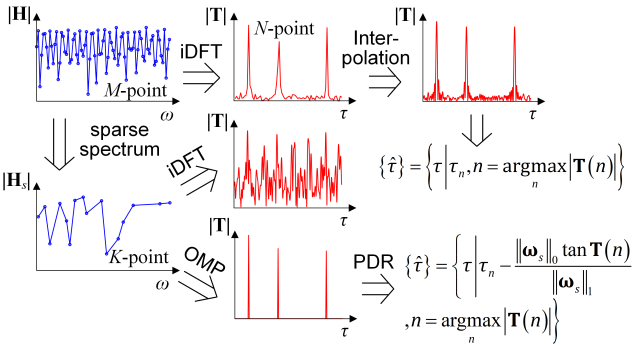

Fig. 2. Comparison of multipath measurement between iDFT-based methods and the proposed OMP-PDR method.

III. Orthogonal Matching Pursuit and Phase-Derived Ranging Combined Sparse I-OFDR

Fortunately, the time-domain response exhibits sparsity due to the limited number of transfer paths, implying that most elements in **T**are zero. Additionally, Fourier basis functions are inherently orthogonal. Therefore, the OMP method can be effectively employed. Let the frequencies of the sparse transfer response be denoted by$\omega_s = [\omega_{s,1}, \omega_{s,2}, \ldots, \omega_{s,k}, \ldots, \omega_{s,K}]^H$. Then the best-matching transfer delay can be estimated by:

$$\begin{aligned} \mathbf{T}(n) &= \underset{\alpha}{\operatorname{argmin}} \left\| \omega_s(\tau_n)\alpha - \mathbf{H}_s \right\|_2 \\ \text{s.t. } n &= \underset{n}{\operatorname{argmax}} \left| \omega_s(\tau_n)^H \mathbf{H}_s \right| \end{aligned} \tag{5}$$

Given that white noise has a significant impact on measurements, (5) provides the best estimate of $\mathbf{T}(n)$ using the least-squares method (LS). Once the best-matching delay is identified, the contribution of $\mathbf{T}(n)$ can be substracted to determine the next best-matching delay. By iterating, all paths can be estimated.

The computational complexity of OMP is $O(L \cdot K \cdot N)$. When measuring long-range transfer delays with high accuracy, the value of N can become exceedingly large. This is because the time-delay interval $\Delta\tau$ in **T** dictates the minimum distinguishable time difference. Under such conditions, the computational overhead can far exceed that of the inverse fast Fourier transform (iFFT), which has a computational complexity of $O(N \cdot \log N)$. Furthermore, the discrete nature of the OMP results makes interpolation challenging. To address this, we integrate the PDR with the OMP algorithm. PDR estimates the optical transfer delay by calculating the slope of the phase response across frequency, enabling measurement accuracy beyond the limit imposed by OMP's fixed interval [14].

Assuming that the accurate transfer delay from one measured path is $\tau_{m,l}$ and the time-domain response obtained from the OMP algorithm is $\mathbf{T}(n)$. In theory, the time-domain response **T** should be a real-valued vector. However, due to the discretization in the time domain, the obtained time-domain result is a projection of $\omega_s(\tau_{m,l})$ onto $\omega_s(\tau_n)$. Based on this projection relationship, we can derive an identity:

$$\frac{\omega_s(\tau_n)^H \cdot \omega_s\left(\tau_{m,l}\right)}{\left|\omega_s(\tau_n)^H \cdot \omega_s\left(\tau_{m,l}\right)\right|} = \frac{\mathbf{T}(n)}{|\mathbf{T}(n)|} \tag{6}$$

Therefore, if the condition $|\tau_{m,l} - \tau_n| < \Delta\tau \ll 1/\|\omega_s\|_\infty$ holds, the PDR can be applied as follows:

$$\begin{aligned} \arg \mathbf{T}(n) &= \arg \sum_{k=1}^{\|\omega_s\|_0} e^{j\omega_{s,k}\left(\tau_n - \tau_{m,l}\right)} \\ &\approx \arg\left\{ \|\omega_s\|_0 + j\left(\tau_n - \tau_{m,l}\right)\|\omega_s\|_1 \right\} \end{aligned} \tag{7}$$

This overall measurement process is illustrated in the third row of Fig. 2. Finally, the estimated transfer delay is given by:

$$\hat{\tau}_{m,l} = \tau_n - \frac{\|\omega_s\|_0}{\|\omega_s\|_1} \tan \mathbf{T}(n) \tag{8}$$

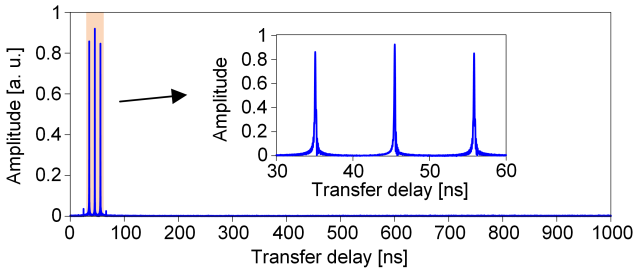

Fig. 3. Time-domain response of three reflected FBG peaks obtained through iDFT.

For the configurations shown in Figs. 1(b) and 1(c), wavelength sensing can be implemented using the following formula:

$$\hat{\lambda}_l = \lambda_l + \frac{\tau_l - \hat{\tau}_{m,l}}{DL} \tag{9}$$

where λ_l and τ_l are the reference wavelength and the corresponding transfer delay, D and L are the dispersion coefficient and the length of the dispersion compensating fiber (DCF).

IV. Experiment Results

Algorithm 1 OMP-PDR Combined Sparse I-OFDR

Input: Transfer response **H**, sparse frequency ω_s, minimum time interval $\Delta\tau$, measurement range τ_{max}, and path number L.

Output: Estimated multipath delay $[\tau_{m,l} | l = 1, 2, .., L]$

1. Compute $\omega_s(\tau_n)$ for $1 \le n \le N$ according to (3), where $\tau_n = (n-1)\tau_{max}/\Delta\tau$
2. $\Omega_s(\tau)$=[$\omega_s(\tau_1)$, $\omega_s(\tau_2)$,..., $\omega_s(\tau_N)$]
3. Φ =Ø, **T**= 0
4. **for** l = 1, 2,..., L, **do**
5. n =argmax$_n$|$\Omega_s(\tau_n)^H \cdot$ **r**$_{l-1}$|, $\Phi_l = \Phi_{l-1} \cup \Omega_s(\tau_n)$
6. **T**=$(\Phi^H \cdot \Phi)^{-1}\Phi^H$·**H**, **r**$_l$ =**H**−Φ·**T**
7. $\tau_{m,l} = \tau_n$−tan[arg(**T**(n))]·$|\omega_s\|_0/\|\omega_s\|_1$
8. end for

To validate the proposed OMP-PDR method, we conducted distributed FBG sensing and multi-wavelength demodulation experiments. The experimental setups are depicted in Figs. 1(b) and 1(c). In these experiments, we employed an MZM (Fujitsu, FTM7938EZ) with a rate for 40 Gbit/s and a PD (Discovery40S) featuring a 3-dB bandwidth of 20 GHz. A DCF with a total dispersion of –460.6 ps/nm was utilized to convert wavelength variations into transfer delay shifts. Additionally, a commercial VNA (Keysight, N5235A), capable of operating at a frequency up to 40 GHz, was used as both the RF source and receiver.

In the strain sensing experiment, three FBGs with distinct center wavelengths (1498.23 nm, 1550.18 nm, and 1552.64 nm) and a reflectivity of 99% are connected along the same fiber. The separation between these FBGs is approximately 1 m. The VNA is configured to sweep frequencies from 3 GHz to 13 GHz in steps of 1 MHz. Fig. 3 illustrates the time-domain response calculated using the iDFT. The third FBG is subjected to strain ranging from 0 $\mu\varepsilon$ to 500 $\mu\varepsilon$ in increments of 50 $\mu\varepsilon$. To employ the proposed OMP-PDR method to demodulate the

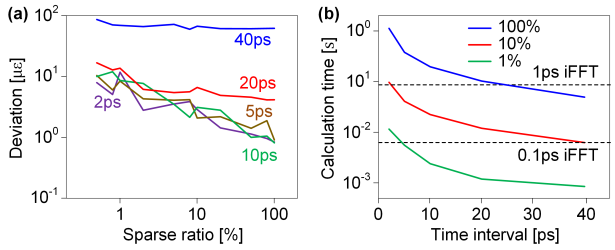

Fig. 4. Experimental results of FBG strain sensing. (a) The influence of the sparse ratio and time-delay interval on strain deviation. (b) Computational time comparison between the proposed method and the iFFT approach.

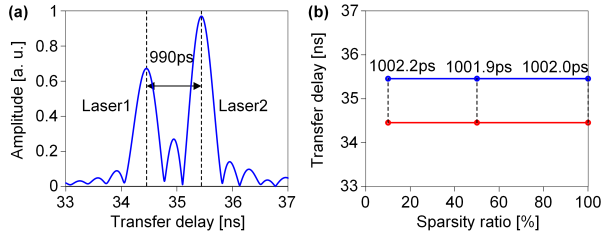

Fig. 5. Experimental results of multi-wavelength demodulation. (a) Time-domain response derived from the iFFT. (b) Transfer delay of the two lasers measured using the proposed method.

strain, we select the frequency points randomly. The results are presented in Fig. 4. The sparsity ratio is defined as the ratio of the number of chosen frequency points for OMP to the total number of frequency points. As shown in Fig. 4(a), the sensing deviation exhibits a trend similar to the sparsity ratio when the time-delay interval is set below 10 ps. This phenomenon can be attributed to the application of the first-order Taylor approximation, $\exp(x) \approx 1+x$, in (7). Given the maximum frequency of 13 GHz, this approximation introduces a phase error exceeding than 0.1 rad when the time-delay interval exceeds 10 ps. With a time-delay interval of 10 ps and a sparsity ratio of 10%, the strain deviation remains at approximately 2.8 $\mu\varepsilon$.

We also compare the computational overhead of our method with that of the iFFT. The calculations are performed on a 13th-Gen Intel[1] Core[2] i5-13500H CPU. As depicted in Fig. 4(b), the computational time scales linearly with the sparsity ratio, consistent with the theoretical computational complexity $O(L \cdot K \cdot N)$. For a time-delay interval of 10 ps and a sparsity ratio of 10%, the computational time is approximately 20 ms. In contrast, the iFFT method requires 86 ms when using a 0.1 ps time-delay interval (corresponding to a strain resolution of 0.53 $\mu\varepsilon$), which is significantly longer than our method. While reducing the time-delay interval to 1 ps in the iFFT, it compromises strain resolution, resulting in a value greater than 5.3 $\mu\varepsilon$. It means that the iFFT method has an inherent trade-off between accuracy and time consumption.

In the multi-wavelength demodulation experiment, the VNA is configured to sweep frequencies from 14 GHz to 17 GHz in steps of 300 kHz. Two tunable lasers (Tunics, T100S-HP) are set at wavelengths of 1550 nm and 1552.17 nm. Based on the group delay dispersion of -460.2 nm/ps, the theoretical transfer delay difference between the two lasers is calculated to be 1.0 ns. Fig. 5 presents the results obtained from the iFFT and the proposed method. As illustrated, the time-delay difference derived from iFFT is 990 ps, whereas the measured transfer delay using the proposed method is approximately 1002 ps. The enhanced accuracy of the proposed method can be attributed to the fact that the side lobes generated from the Fourier analysis are suppressed. The proposed method maintains consistent measurement accuracy across sparsity ratios ranging from 10% to 100% in the experiment.

[1]Registered trademark.

[2]Trademarked.

V. Conclusion

An I-OFDR demodulation method based on OMP and PDR is proposed to significantly reduce system overhead by leveraging the sparse RF transfer response. Experimental results demonstrate an accuracy of 2.8 $\mu\varepsilon$ in distributed FBG strain sensing with an RF transfer response with sparsity ratio of 10%. The computational overhead of the OMP algorithm is further minimized through the application of the PDR technique. When interrogating the wavelengths of the two lasers, the proposed method exhibits enhanced measurement accuracy compared to the traditional iFFT approach. Given its reduced overhead, the OMP-PDR method holds significant potential for a wide range of distributed sensing applications.

References

[1] I. Ashry et al., "A review of distributed fiber–optic sensing in the oil and gas industry," *J. Lightw. Technol.*, vol. 40, no. 5, pp. 1407–1431, Dec. 25, 2022.

[2] B. Glisic and D. Inaudi, "Development of method for in-service crack detection based on distributed fiber optic sensors," *Structural Health Monitor.*, vol. 11, no. 2, pp. 161–171, Mar. 2012.

[3] X. Jiang, X. Wang, A. Zhao, J. Yao, and S. Pan, "A multi-antenna GNSS-over-fiber system for high accuracy three-dimensional baseline measurement," *J. Lightw. Technol.*, vol. 37, no. 17, pp. 4201–4209, Jun. 10, 2019.

[4] J. Yao, "Microwave photonic sensors," *J. Lightw. Technol.*, vol. 39, no. 12, pp. 3626–3637, Dec. 25, 2020.

[5] L. Wang et al., "Single-shot optical transfer delay measurement with sub-picosecond accuracy and sub-millisecond range," *Photon. Res.*, vol. 13, no. 5, pp. 1302–1312, 2025.

[6] J. Clement, H. Maestre, G. Torregrosa, and C. R. Fernández-Pousa, "Incoherent optical frequency-domain reflectometry based on homodyne electro-optic downconversion for fiber–optic sensor interrogation," *Sensors*, vol. 19, no. 9, p. 2075, May 2019.

[7] J. Clement, G. Torregrosa, J. Hervás, D. Barrera, S. Sales, and C. R. Fernández-Pousa, "Interrogation of a sensor array of identical weak FBGs using dispersive incoherent OFDR," *IEEE Photon. Technol. Lett.*, vol. 28, no. 10, pp. 1154–1156, Feb. 29, 2016.

[8] D. Zheng, X. Zhang, X. Zou, and W. Pan, "High-resolution microwave photonic filtering interrogation technology based on time-domain refined analysis," in *Proc. Asia Commun. Photon. Conf. (ACP)*, Shenzhen, China, Nov. 2022, pp. 1848–1851.

[9] J. Wang et al., "Interrogation of a large-capacity densely spaced fiber Bragg grating array using chaos-based incoherent-optical frequency domain reflectometry," *Opt. Lett.*, vol. 44, no. 21, pp. 5202–5205, 2019.

[10] L. Wang, L. Ren, X. Wang, and S. Pan, "Time-resolution enhanced multi-path OTD measurement using an adaptive filter based incoherent OFDR," *Chin. Opt. Lett.*, vol. 22, no. 1, 2024, Art. no. 013901.

[11] J. C. Bellido et al., "Fast incoherent OFDR interrogation of FBG arrays using sparse radio frequency responses," *J. Lightw. Technol.*, vol. 36, no. 19, pp. 4393–4400, Mar. 30, 2018.

[12] S. Werzinger, M. Gottinger, S. Gussner, S. Bergdolt, R. Engelbrecht, and B. Schmauss, "Model-based compressed sensing of fiber Bragg grating arrays in the frequency domain," in *Proc. 25th Opt. Fiber Sensors Conf. (OFS)*, Apr. 2017, pp. 1–4.

[13] J. A. Tropp and A. C. Gilbert, "Signal recovery from random measurements via orthogonal matching pursuit," *IEEE Trans. Inf. Theory*, vol. 53, no. 12, pp. 4655–4666, Dec. 2007.

[14] S. Li et al., "Optical fiber transfer delay measurement based on phase-derived ranging," *IEEE Photon. Technol. Lett.*, vol. 31, no. 16, pp. 1351–1354, Jun. 3, 2019.